Proceedings of the ASME 2010 3rd Joint US-European Fluids Engineering Summer Meeting and 8th International Conference on Nanochannels, Microchannels, and Minichannels
FEDSM-ICNMM2010
August 1-5, 2010, Montreal, Canada

FEDSM-ICNMM2010-30113

THE LBM RESEARCH ON TRANSVERSE-AXIS ROTARY VISCOUS PUMP

Fan YANG, Haimin WANG, Eryun CHEN, Lianguo LIU
School of Energy & Power Engineering, University of Shanghai for Science and Technology
Shanghai, China
Email:usstyf@126.com

ABSTRACT

In this study, the flow pattern in the novel viscous pump is analyzed using the lattice Boltzmann method (LBM) to simulate the whole flow field in the pump with three shape cross-sections of cylinders, the circular, rectangular, as well as square. The solid curved wall boundary condition based on interpolation and bounce-back on the wall of the LBM simulation is used in steady and unsteady flow, and the moving boundary condition is also used in the latter. The analyses predicted the distributions of streamlines and the average dimensionless velocities at the exit profile which change with time. The numerical results of the average dimensionless velocities at the exit profile are in agreement with previous experimental works, which indicate that the circular contour is better than the rectangular or square ones.

INTRODUCTION

Interest in the fluid mechanics of micromachines has been boosted by recent impressive advances in the technology of microfabrication. There are certain physical effects that become important at these small scales which have to be taken into account in the design of appropriate machinery. Large viscous forces in relation to inertia are one effect. Due to these differences, micromachines that are simple reduced in size may not work.

From the point of view of application, pumps are one of the kinds of fluid micromachines that have been conceived. At such small scales, conventional principles of rotating turbomachinery based on centrifugal and inertial forces are not very useful. Reciprocating pumps, though feasible, require rather intricate microfabrication on account of the need for valves and seals. Since viscous forces tend to be important at small scales, a pump based on viscous action seems to be logical [1-4].

The lattice Boltzmann method, a derivative of lattice gas automata (LGA) method, has been successfully demonstrated to be an alternative numerical scheme to traditional numerical methods for solving partial differential equations and modeling physical systems, particularly for simulating fluid flows with the Navier-Stokes equations. In traditional numerical methods, the Navier-Stokes equations are solved by some specific numerical discretization. In contrast, the fundamental principle of lattice Boltzmann method is to construct a simplified molecular dynamic that incorporates the essential characteristics of the physical microscopic processes so that the macroscopic averaged properties obey the desired macroscopic equations. This microscopic approach in the lattice Boltzmann method incorporates several advantages of kinetic theory. It includes clear physical pictures, easy implementation of boundaries and fully parallel algorithms [5-6]. In particular, the Lattice Boltzmann method has been successfully applied to problems such as fluid flows through porous media [7], multiphase fluid flows [8], and suspension motions in fluids [9-11].

TRANSVERSE-AXIS ROTARY VISCOUS PUMP AND DESIGN PRINCIPLES

Pumping devices, which is appropriate for microscale applications, can be divided into two mean categories: mechanical pumps and nonmechanical pumps [2].

The first category usually utilizes moving parts such as check valves, oscillating membranes, or turbines for delivering a constant fluid volume in each pump cycle. The second category adds momentum to the fluid for pumping effect by converting another energy form into the kinetic energy. While the first category was mostly used in macroscale pumps and the micropumps with relatively large size and large flow rates, the second category discovers its advantages in the microscale. Since the viscous force in microchannels increase in the second order with the miniaturization, the first pump category cannot deliver enough power in order to overcome its high fluidic impedance.

The transverse-axis rotary viscous pump is the type of mechanical pumps. It is based on the rotation of a cylinder placed asymmetrically in a narrow duct; the differential viscous resistance between the small and large gaps causes a net flow along the channel.

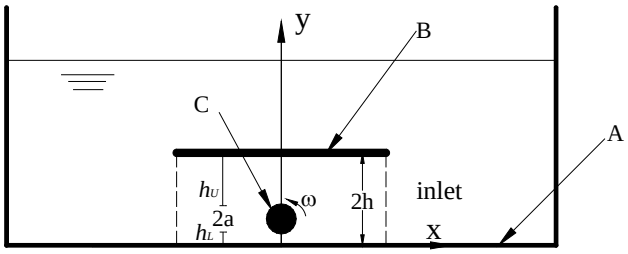

Fig. 1 Schematic of flow configuration

Fig. 1 shows the geometrical configuration of the problem under investigation. The plate **B** is positioned at a vertical distance 2*h* from the bottom of the open tank **A** filled with a viscous fluid. A cylindrical rotor **C** (with the largest distance 2*a* of cross-section) is placed at distance h_U and h_L from the plate **B** and the bottom of the tank, respectively. In the present configuration, fluid flow from right to left in the channel portion is induced by counter-clockwise rotation of the cylinder. The space within the channel walls, indicated by the dashed line, as the pump portion; the rest will be a lord external to the pump.

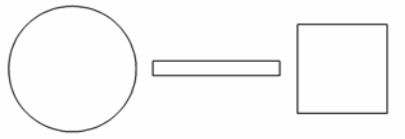

Fig. 2 Three type cross-sections of cylinders

Fig. 2 shows the three shape cross-sections of cylinders, the circular (8.98 mm diameter), square (8.98 mm diagonal) and rectangular (8.98 mm×1 mm). The latter two shapes are unsteady as well as moving boundary problem.

Some parameters of pump are defined below:

Dimensionless length $s = h/a$

Dimensionless velocity $\boldsymbol{U}' = \boldsymbol{u}/\omega a$

Eccentricity $\varepsilon = (h_U + a - h)/2a$

Reynolds number $Re = 2\omega a^2/\nu$

GENERAL LBGK MODEL

A popular kinetic model adopted in the literature is the single-relaxation-time (SRT) approximation, the so-called Bhatnagar-Gross-Krook (BGK) model [12]

$$\frac{\partial f}{\partial t} + \boldsymbol{\xi}\cdot\nabla f = -\frac{1}{\lambda}(f - f^{(0)}) \tag{1}$$

where $f^{(0)}$ is equilibrium distribution function (the Maxwell-Boltzmann distribution function), and λ is the relaxation time.

To solve for *f* numerically, Eq. (1) is first discretized in the velocity space using a finite set of velocity vectors $\{\boldsymbol{\xi}_\alpha\}$ in the context of the conservation laws:

$$\frac{\partial f_\alpha}{\partial t} + \boldsymbol{\xi}_\alpha\cdot\nabla f_\alpha = -\frac{1}{\lambda}(f_\alpha - f_\alpha^{(eq)}) \tag{2}$$

In the above equation, $f_\alpha(\boldsymbol{x},t) \equiv f(\boldsymbol{x},\boldsymbol{\xi}_\alpha,t)$ is the distribution function associated with the αth discrete velocity $\boldsymbol{\xi}_\alpha$ and $f_\alpha^{(eq)}$ is the corresponding equilibrium distribution function in the discrete velocity space. The nine-velocity square lattice model, being referred to as the 2-D 9-velocity (D2Q9) model (Fig. 3), has been widely and successfully used for simulating two-dimensional (2-D) flows. In the D2Q9 model, $\boldsymbol{e}_\alpha$ denotes the discrete velocity set,

$$\boldsymbol{e}_\alpha = \begin{Bmatrix} 0 & 1 & -1 & 0 & 0 & 1 & -1 & -1 & 1 \\ 0 & 0 & 0 & 1 & -1 & 1 & -1 & 1 & -1 \end{Bmatrix} c \tag{3}$$

where $c = \delta x/\delta t$, δx and δt are the lattice constant and the time step size, respectively. The equilibrium distribution for D2Q9 model is of the form [13]

$$f_\alpha^{(eq)} = \omega_\alpha \rho[1 + \frac{3}{c^2}(\boldsymbol{e}_\alpha\cdot\boldsymbol{u}) + \frac{9}{2c^4}(\boldsymbol{e}_\alpha\cdot\boldsymbol{u})^2 - \frac{3}{2c^2}\boldsymbol{u}\cdot\boldsymbol{u}] \tag{4}$$

where ω_α is the weighting factor given by

$$\omega_\alpha = \begin{cases} 4/9 & \alpha = 0 \\ 1/9 & \alpha = 1,2,3,4 \\ 1/36 & \alpha = 5,6,7,8 \end{cases} \tag{5}$$

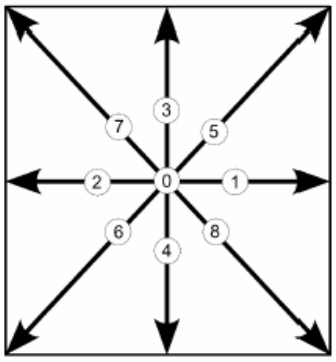

Fig. 3 A 2-D 9-velocity lattice (D2Q9) model

In the discretized velocity space, the density ρ and momentum fluxes $\rho\boldsymbol{u}$ are defined as particle velocity moments of the distribution function,

$$\rho = \sum_{\alpha=0}^{8} f_\alpha, \quad \rho\boldsymbol{u} = \sum_{\alpha=0}^{8} \boldsymbol{e}_\alpha f_\alpha \tag{6}$$

The speed of sound in this model is $c_s = c/\sqrt{3}$ and the equation of state is that of an ideal gas,

$$p = \rho c_s^2 \tag{7}$$

In the LBM, Eq. (2) is discretized in a very special manner. The completely discretized equation, with the time step δt and space step $\delta x = \boldsymbol{e}_\alpha \delta t$, is

$$f_\alpha(\boldsymbol{x}_i + \boldsymbol{e}_\alpha\delta t, t + \delta t) - f_\alpha(\boldsymbol{x}_i, t) = -\frac{1}{\lambda}[f_\alpha(\boldsymbol{x}_i,t) - f_\alpha^{(eq)}(\boldsymbol{x}_i,t)] \tag{8}$$

where $\tau = \lambda/\delta t$, and $\boldsymbol{x}_i$ is a point in the discretized physical space. Eq. (9), termed the LBE with BGK approximation or LBGK model, is usually solved in the following two steps:
collision step:

$$\tilde{f}_\alpha(\boldsymbol{x}_i, t+\delta t) = f_\alpha(\boldsymbol{x}_i, t) - \frac{1}{\lambda}[f_\alpha(\boldsymbol{x}_i, t) - f_\alpha^{(eq)}(\boldsymbol{x}_i, t)] \quad (9a)$$

streaming step:

$$f_\alpha(\boldsymbol{x}_i + \boldsymbol{e}_\alpha \delta t, t+\delta t) = \tilde{f}_\alpha(\boldsymbol{x}_i, t+\delta t) \quad (9b)$$

where $\tilde{f}$ represents the post-collision state.

In order to derive the Navier-stokes equations from LBE, the Chapman-Enskog expansion is used. The corresponding viscosity in the Navier-stokes equation derived from Eq. (8) is

$$\nu = \frac{2\tau - 1}{6} \quad (10)$$

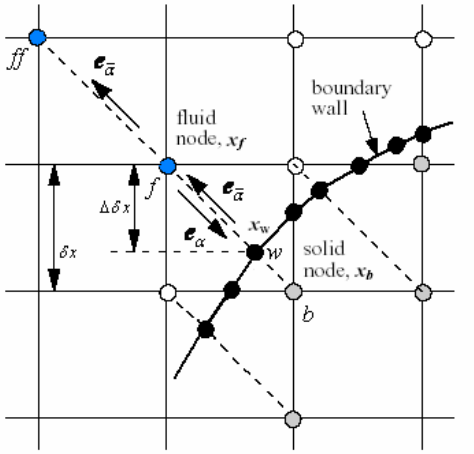

Fig. 4 Layout of the regularly spaced lattices and curved wall boundary

SOLID BOUNDARY TREATMENT AND MOVING BOUNDARY CONDITION OF LBM

Chronologically, LBM was evolved from the LGA method. In dealing with straight walls, the bounce-back condition was proposed in conjunction with the LGA method. Curved walls were treated as a series of steps. This method has been extensively used in LBM simulation. Only more recently, efforts have been made to preserve the geometric integrity of the curved walls which is important in simulating high Reynolds flows.

In Fig. 4, a curved wall separates the solid region from the fluid region. The lattice node on the fluid side of the boundary is denoted as $\boldsymbol{x}_f$ and that on the solid side is denoted as $\boldsymbol{x}_b$. The filled small circles on the boundary, $\boldsymbol{x}_w$, denote the intersections of the wall with various lattice links. The boundary velocity at $\boldsymbol{x}_w$ is $\boldsymbol{u}_w$. The fraction of an intersected link in the fluid region is Δ, that is,

$$\Delta = \frac{|\boldsymbol{x}_f - \boldsymbol{x}_w|}{|\boldsymbol{x}_f - \boldsymbol{x}_b|}, \quad 0 \le \Delta \le 1 \quad (11)$$

The horizontal or vertical distance between $\boldsymbol{x}_b$ and $\boldsymbol{x}_w$ is $\Delta\delta x$ on the square lattice. The particle momentum moving from $\boldsymbol{x}_f$ to $\boldsymbol{x}_b$ is $\boldsymbol{e}_\alpha$ and the reversed one from $\boldsymbol{x}_b$ to $\boldsymbol{x}_f$ is $\boldsymbol{e}_{\bar{\alpha}} = -\boldsymbol{e}_\alpha$.

Second-order Accuracy Models for Curved Walls

Filippova and Hänel [14] presented a curved boundary condition which, for the first time, provided a second-order accurate treatment for a curved solid wall. To improve the numerical stability, Mei *et al.* [15] presented an improved curved boundary condition based on the scheme of Filippova and Hänel. Bouzidi *et al.* [16] proposed a different but simple boundary condition for curved wall based on interpolation and the bounce-back scheme.

To construct $\tilde{f}_{\bar{\alpha}}(\boldsymbol{x}_b, t)$ based upon known information in the surrounding fluid nodes, Filippova and Hänel [14] proposed the following linear interpolation:

$$\tilde{f}_{\bar{\alpha}}(\boldsymbol{x}_b, t) = (1-\chi)\tilde{f}_{\bar{\alpha}}(\boldsymbol{x}_f, t) + \chi f_\alpha^{(*)}(\boldsymbol{x}_b, t) + 2\omega_\alpha \rho \frac{3}{c^2}\boldsymbol{e}_\alpha \cdot \boldsymbol{u}_w \quad (12)$$

with

$$f_\alpha^{(*)}(\boldsymbol{x}_b, t) = \omega_\alpha \rho(\boldsymbol{x}_f, t)[1 + \frac{3}{c^2}\boldsymbol{e}_\alpha \cdot \boldsymbol{u}_{bf} + \frac{9}{2c^4}(\boldsymbol{e}_\alpha \cdot \boldsymbol{u}_f)^2 - \frac{3}{2c^2}\boldsymbol{u}_f \cdot \boldsymbol{u}_f] \quad (13)$$

In the above, $\boldsymbol{u}_f \equiv \boldsymbol{u}(\boldsymbol{x}_f, t)$ is the fluid velocity near the wall and $\boldsymbol{u}_{bf}$ is to be chosen.

$$\boldsymbol{u}_{bf} = \frac{(\Delta-1)\boldsymbol{u}_f}{\Delta} + \frac{\boldsymbol{u}_w}{\Delta} \text{ and } \chi = (2\Delta - 1)/\tau \text{ for } \Delta \ge 0.5 \quad (14a)$$

$$\boldsymbol{u}_{bf} = \boldsymbol{u}_f \text{ and } \chi = \frac{(2\Delta-1)}{(\tau-1)} \text{ for } \Delta < 0.5 \quad (14b)$$

This scheme was used in the simulation of flow over asymmetrically placed cylinder in the channel flow.

Mei *et al.* [15] suggested using different nodes to obtain $\tilde{f}_{\bar{\alpha}}(\boldsymbol{x}_b, t)$ when $\Delta < 1/2$. The purpose was to improve the numerical stability over Filippova and Hänel's scheme. Thus, Eq. (14b) was replaced by

$$\boldsymbol{u}_{bf} = \boldsymbol{u}_{ff} \text{ and } \chi = \frac{(2\Delta-1)}{(\tau-1)} \text{ for } \Delta < 0.5 \quad (15)$$

where $\boldsymbol{u}_{ff}$ is the fluid velocity at the *ff* node in figure 4.

Bouzidi *et al.* [16] presented a simpler boundary condition based on the bounce-back for the wall located at arbitrary position. In their work, both linear scheme and the quadratic schemes were given to obtain $f_{\bar{\alpha}}(\boldsymbol{x}_f, t+\delta t)$ which is equivalent to $\tilde{f}_{\bar{\alpha}}(\boldsymbol{x}_b, t)$. The linear version was as follow:

$$f_{\bar{\alpha}}(\boldsymbol{x}_f, t+\delta t) = \frac{1}{2\Delta}\tilde{f}_\alpha(\boldsymbol{x}_f, t) + \frac{2\Delta-1}{2\Delta}\tilde{f}_{\bar{\alpha}}(\boldsymbol{x}_f, t)$$

for $\Delta \ge 0.5$ (16a)

$$f_{\bar{\alpha}}(\boldsymbol{x}_f, t+\delta t) = 2\Delta\tilde{f}_\alpha(\boldsymbol{x}_f, t) + (1-2\Delta)\tilde{f}_\alpha(\boldsymbol{x}_f - \boldsymbol{e}_\alpha \delta t, t)$$

for $\Delta < 0.5$ (16b)

In the above, it is noted that $\boldsymbol{x}_f - \boldsymbol{e}_\alpha \delta t$ is at the *ff* node in Fig. 4. They computed flow over a 2-D periodical array of cylinders and reported the second-order convergent results for

the inverse of the permeability.

The above three boundary condition treatments all have second-order accuracy for curved boundary. The difference is that the first two needs to construct a fictitious fluid point inside the solid wall, and perform a collision step at that node, while the scheme of Bouzidi *et al*. only requires the known values of f_α on the fluid side and no additional collision is required. It is emphasized that all three methods need to treat the boundary condition separately for $\Delta \geq 0.5$ and $\Delta < 0.5$.

In this paper, the solid curved wall boundary scheme of Bouzidi *et al*. was used to simulate flow within viscous pump for its simple form as well as good computational stability.

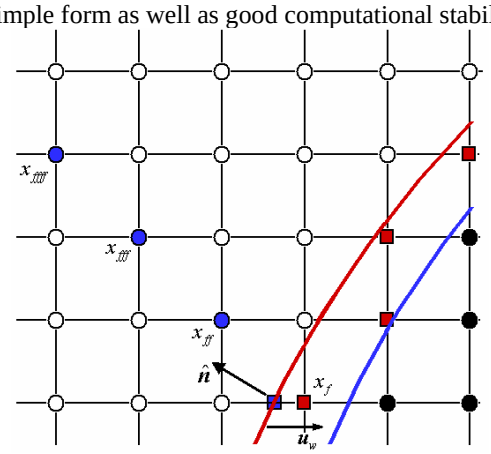

Fig. 5 Scheme of moving boundary condition in LBM

Moving Boundary Condition for Unsteady Flow

Using LBM, solid region is separated from fluid region by walls. When walls are moving with velocity $\boldsymbol{u}_w$, some nodes will move out of the solid region into the fluid region, it must be specified some number of unknown distribution function on these nodes. Referring to Fig. 5, $\boldsymbol{x}_f$ denotes node becoming fluid node from solid region at one time step δt. In this paper, the extrapolation formula proposed by Lallemand *et al*. [17] is used to compute the unknown distribution functions

$$f_\alpha(\boldsymbol{x}_f) = 3f_\alpha(\boldsymbol{x}_{ff}) - 3f_\alpha(\boldsymbol{x}_{fff}) + f_\alpha(\boldsymbol{x}_{ffff}) \qquad (17)$$

where α is the direction which maximizes the quantity $\boldsymbol{e}_\alpha \bullet \hat{\boldsymbol{n}}$, and $\hat{\boldsymbol{n}}$ is the out-normal vector of the wall at the point through which the node moves to fluid region.

NUMERICAL SIMULATION OF TRANSVERSE-AXIS ROTARY VISCOUS PUMP

In this paper, the two-dimensional transverse-axis rotary viscous pump flow at Reynolds number of 0.56, dimensionless length *S* of 1.78, and eccentricity of 0.17 are simulated with LBM method described above, and the results are compared with experimental works reported previous.

Computation Region, Grid and Boundary Condition

The present simulation uses square grids with 978×110 lattice units to whole tank, while each lattice unit corresponds to 0.5 mm. The interpolation and bounce-back is used to solid curved wall, and the bounce-back boundary conditions are used at other walls. The shear-free boundary condition is used in free surface of tank.

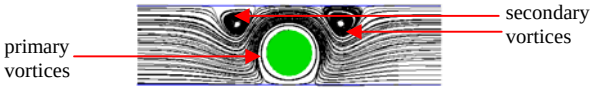

Fig.6 Streamlines of circular rotary axes

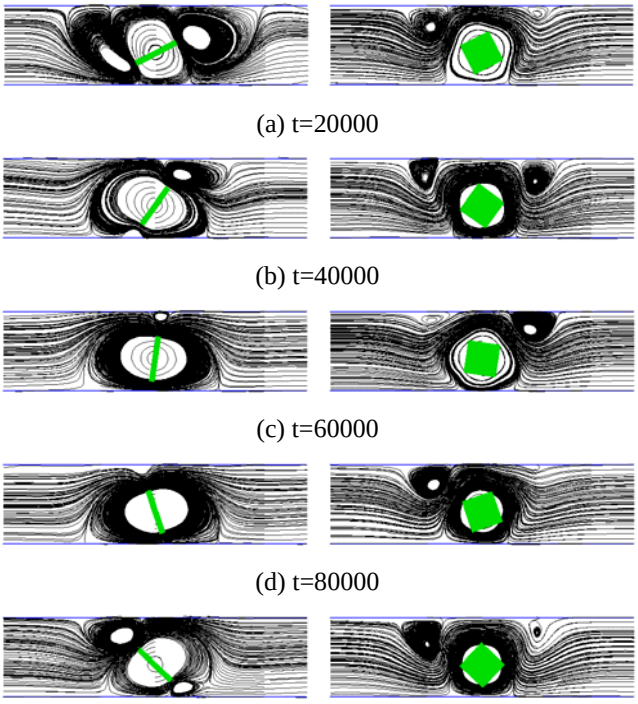

(a) t=20000

(b) t=40000

(c) t=60000

(d) t=80000

(e) t=100000

Fig.7 Instantaneous streamlines of non-circular rotary axes

Simulation Results and Analyses

1. Distributions of stream lines in pump

Fig.6 and Fig.7 show the streamlines in viscous pump with circular/non-circular rotary axes. The primary vortices are formed around cylinder, at the meanwhile, other two secondary vortices exist. The size and location of vortices varies with the shape of cylinder section. The more symmetry of cylinder cross-section, the smaller of primary vortices size is.

2. Evolvement history of average dimensionless velocity at outlet profile

Fig. 8 shows the evolvement history of average dimensionless velocity at outlet profile of three shape cross-section rotary axes. The tendency of the evolvement is similar, and non-circular cross-section rotary axis fluctuates periodically due to its moving boundary. However, the more symmetry of cylinder is, the large value of dimensionless velocity is.

3. Comparison of computational and experimental results of average dimensionless velocity

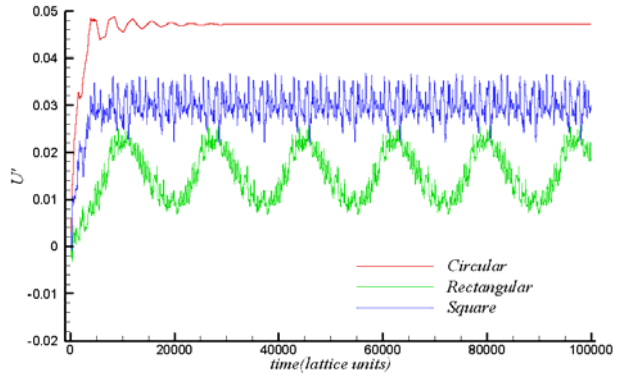

Fig.8 Evolvement history of average dimensionless velocity at outlet profile of three shape cross-section rotary axes

Table.1 Computational and experimental results of average dimensionless velocity

U'	Computational	Experimental[3]
circular	0.0472	0.046
rectangular	32.52%	31.8%
square	63.46%	64.4%

The computational and experimental results reported are listed in Table 1. For non-circular axes, it is the phase-average value in last three periods before computation finished. It can be viewed that the both two results are in agreement with each other, which indicate that the circular contour is better than the rectangular or square ones.

CONCLUSION

In this paper, a transverse-axis rotary viscous pump is described. The lattice Boltzmann method simulations are carried out to study the influence of various geometric parameters, which the results are compared with the experiment ones reported previous. The solid curved wall boundary condition based on interpolation and bounce-back on the wall of the LBM simulation was used in steady and unsteady flow, and the moving boundary condition is also used in the latter. The numerical results indicated that the more effective pumping and better performance is obtained with the increase symmetry of cylinder cross-section.

Being a derivative of kinetic method, LBM has the several advantages on solving problems of unsteady and moving boundary, and will be getting extensive application in future with the progress of computational technique.

ACKNOWLEDGMENTS

Project supported by the National Natural Science Foundation of China (Grant Nos. 10902070, 50976072), the Special Scientific Foundation for Selection and Cultivation of Excellent Young Scholars in Shanghai (Grant No. slg09002) and the Leading Academic Discipline Project of Shanghai Municipal Education Commission (Grant No. J50501).

REFERENCES

[1] Gad-el-Hak M. The fluid mechanics of microdevices-The freeman scholar lecture [J]. ASME Journal of Fluids Engineering, 1999, 121: 5-33.

[2] Nguyen NT, Huang X, Chuan T. MEME-micropumps: a review [J]. ASME Journal of Fluids Engineering, 2002, 124: 384-392.

[3] Sen M, Wajerski D, Gad-el-Hak M. A novel pump for MEMS applications [J]. ASME Journal of Fluids Engineering, 1996, 118: 624-627.

[4] Sharatchandra M C, Sen M, Gad-el-Hak M. Navier-Stokes simulations of a novel viscous pump [J]. ASME Journal of Fluids Engineering, 1997, 119: 372-382.

[5] Qian Y, d'Humières D, Lallemand P. Lattice BGK models for Navier-Stokes equation [J]. Europhysics Letters, 1992, 17: 479-484.

[6] Chen S, Doolen G D. Lattice Boltzmann method for fluid flows [J]. Annual Review of Fluid Mechanics, 1998, 30: 329-364.

[7] Spaid M A A, Phelan F R Jr. Lattice Boltzmann methods for modeling microscale flow in fibrous porous media [J]. Physics of Fluids, 1997, 9: 2468-2474.

[8] Grunau D, Chen S, Eggert K. A lattice Boltzmann model for multiphase fluid flows [J]. Physics of Fluids A, 1993, 5: 2557-2562.

[9] Shan X, Chen H. Lattice Boltzmann Model for simulating flows with multiple phases and components [J]. Physical Review E, 1993, 47(3): 1815-1819.

[10] Ladd A J C. Numerical simulations of particulate suspensions via a discretized Boltzmann equation. Part. 1. Theoretical foundation [J]. Journal of Fluid Mechanics, 1994, 271: 285-309.

[11] Ladd A J C. Numerical simulations of particulate suspensions via a discretized Boltzmann equation. Part 2: Numerical results [J]. Journal of Fluid Mechanics, 1994, 271:311-339.

[12] Bhatnagar P L, Gross E P, Krook M. A model for collision processes in gases. I: Small amplitude processes in charged and neutral one-component system [J]. Physical Review, 1954, 94: 511-525.

[13] Frisch U, Hasslacher B, Pomeau Y. Lattice-gas automata for the Navier-Stokes equations [J]. Physical Review Letters, 1986, 56: 1505-1508.

[14] Filippova O, Hänel D. Grid refinement for lattice-BGK models [J]. Journal of Computational Physics, 1998, 147, 219-228.

[15] Mei R, Luo L, Shyy W. An accurate curved boundary treatment in the lattice Boltzmann method [J]. Journal of Computational Physics, 1999, 155, 307-330.

[16] Bouzidi M, Firdaouss M, Lallemand P. Momentum transfer of a lattice Boltzmann fluid with boundaries [J]. Physics of Fluids. 2001, 13: 3452-3459.

[17] Lallemand P, Luo L. Lattice Boltzmann method for moving boundaries [J]. Journal of Computational Physics, 2003, 184: 406-421.